Modeling of the Magnetic Field in a Vacuum Arc Remelting furnace using the COMSOL Multiphysics® simulation software

V. BRUYERE[1], P.NAMY[1], I.CRASSOUS[2], F.ALEX[2] and C.DEVILLE-CAVELLIN[2]
1. SIMTEC, 5 rue Felix Poulat 38000 GRENOBLE France
2. FRAMATOME, 60 Avenue Paul Girod, 73400 Ugine France

Introduction

The vacuum arc remelting is a refining process used to melt very reactive metals with high melting temperature like titanium Tf(Ti) = 1668°C, zirconium Tf(Zr) = 1852°C or hafnium Tf(Hf) = 2233°C [1]. Melting is performed under vacuum to avoid reactions between the liquid metal and the atmosphere and to purify volatiles compounds at high temperature and low pressure. Framatome uses it in particular for production of Zirconium alloys with both chemical and structural homogeneities, dedicated to nuclear or medical fields. A high electric current is applied between this electrode made of raw material and the mold intended to receive the melted metal and an electric arc occurs. It enables the bottom of the electrode to melt and the liquid drops of metal to fill in the copper mold cooled by a counter flow of water and form the purified ingot. The reactor is equipped with coils to apply an electromagnetic stirring in the liquid metal. Indeed, Lorentz forces are created because of the interaction between the magnetic field from the coils and the current flow applied between the electrodes. The control of the process and especially the stirring is essential to ensure quality through a very low segregation and a controlled solidification structure [2, 3]. For this reason, Framatome and Simtec companies have developed the modeling of the magnetic field in a typical industrial vacuum arc remelting furnace using the COMSOL Multiphysics® software. This model is specifically used to check the capacity of the system to ensure an homogeneous magnetic field for different melting parameters of different products.

Theory / Experimental Set-up

The evolution of the calculated magnetic field as a function of process parameters is compared with experimental values. This validation work constitutes a necessary step prior to any predictive use for process optimization. The measurement consists in evaluating the magnetic field induced by the coils for different intensities inside the furnace. The magnetic field is measured at different heights along the vertical axis with a 3-axis Hall Magnetometer THM1176 provided by the MetroLab company. Its range goes from the µT to 14 T, DC to 1 kHz, with ±1% accuracy. It simultaneously measures all three axes of the magnetic field.

The geometry used for COMSOL Multiphysics® calculations is described schematically in Figure 1.

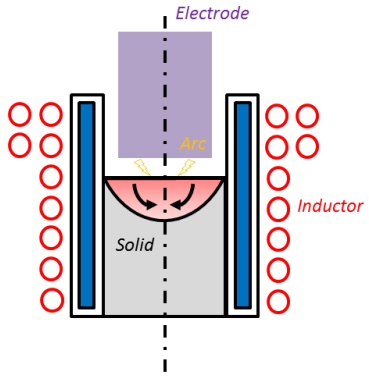

Figure 1: Schematic representation of the geometry. In red, the number of turns of the coils can vary according to z. the purple and grey parts represent the electrode and the ingot in which the current flows.

A more specific figure, zooming on a part of the coils, is provided in Figure 2.

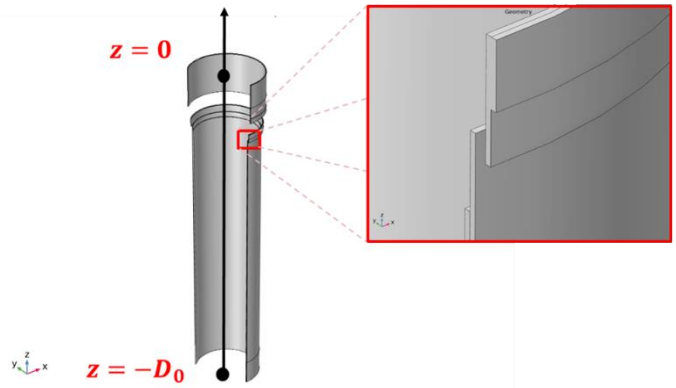

Figure 2. 3D representation of the coils from the 2D axisymmetric model

The coil is modeled in 8 parts, which differs from the others in the number of turns. All these parts are, from an electrical point of view, connected in series, so the intensity is the same.

The exact description of the design of the coils and of their properties are not provided due to confidentiality purpose. For the same reason, the geometrical dimensions have been made a-dimensional, so the length runs from $z = 0$ (top) to $z = -D_0$ (bottom).
The dimensions of the electrode, the ingot and the distance between them will be assumed constant in this work.

Governing Equations / Numerical Model / Simulation / Methods / Use of Simulation Apps

To compute the electro-magnetic field inside the medium, the following Maxwell equations are solved:

In the electrodes and in the arc domain:

$$\nabla \cdot [-\sigma \nabla V] = 0 \qquad \textit{Eq. 1}$$

where V is the electric potential and σ the electrical conductivity of the medium. The electric field $\boldsymbol{E}$ is equal to $-\nabla V$.

A first approach is proposed in this paper, so no plasma is taken into consideration here in the arc domain. The electrical conductivity of the arc is calibrated by adjusting the potential difference between the top and the bottom with experimental data.
In the vacuum, the magnetic field due to the coil is computed though

$$\nabla \times \left(\frac{1}{\mu_0 \, \mu_R} \nabla \times \mathbf{A}\right) + \sigma \nabla V = 0 \qquad \textit{Eq. 2}$$

where $\mu_0 \, \mu_R$ is the magnetic permeability of the material and $\mathbf{A}$ the magnetic vector potential, defined by $\mathbf{B} = \nabla \times \mathbf{A}$.

A Gauge Fixing for A field condition is used to ensure the unicity of the solution:

$$\nabla \cdot \mathbf{A} = 0 \qquad \textit{Eq. 3}$$

The boundary conditions read as follows:

- for the electric current equation in the system, the current density is prescribed on the top boundary of the electrode, and a ground condition potential is used at the bottom ingot to close the mathematical problem,
- for the computation of the magnetic field, each winding coil is described as a homogenized multi-turn coil with the adapted number of turns, the coil wire conductivity and the coil wire section area.

Linear triangular elements are used for meshing. A sensitivity study about the mesh properties has been performed to ensure no-dependency of the solution on the mesh.

Concerning the solver properties, the electric and magnetic fields are computed with the MUMPS direct solver at the stationary state. The damping of the Newton-Rapson method is set to automatic. Due to the linearity of the problem, no numerical difficulty is expected during the computation.

Experimental Results / Simulation Results / Discussion

In order to validate the modeling of the coil, the first part of this work is performed without the electrode and the ingot. Indeed, experimental results were obtained with this configuration. The relative permeability of all materials is set to 1. Consequently, from a magnetic point of view, no effect is expected.
In a second step, the electrode and the ingot are taken into account. The resulting electromagnetic forces are then studied.

Without the electrodes

Figure 3 and Figure 4 describe the components of the magnetic field in the r and z direction, respectively.

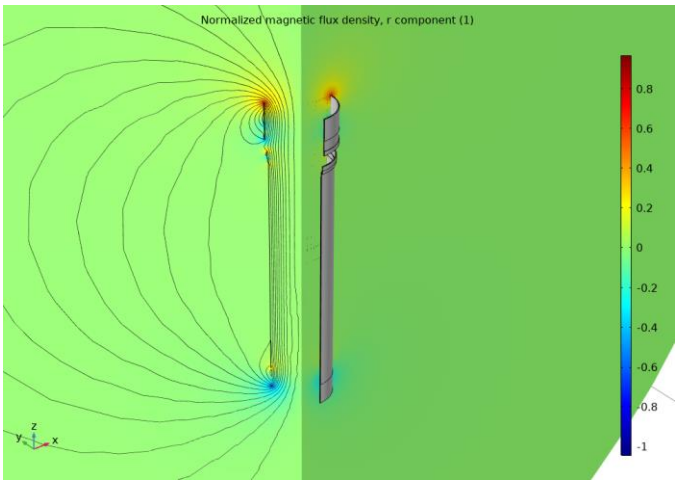

Figure 3. r-component of the non-dimensioned magnetic field

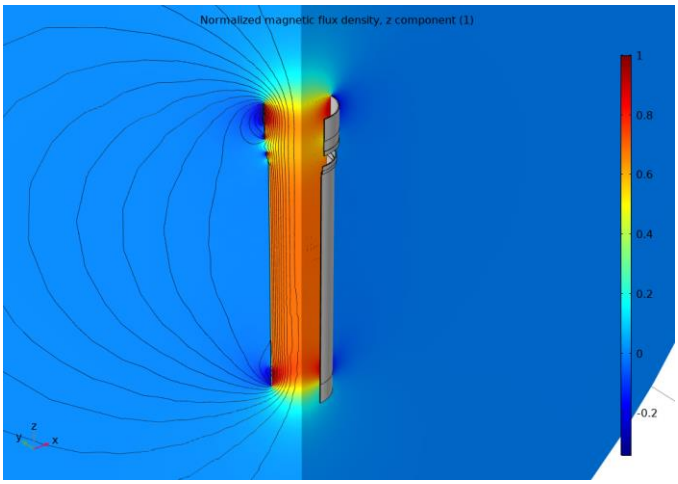

Figure 4. z-component of the non-dimensioned magnetic field

As seen in Figure 5, the norm of the magnetic field is higher at the extremities of the furnace.

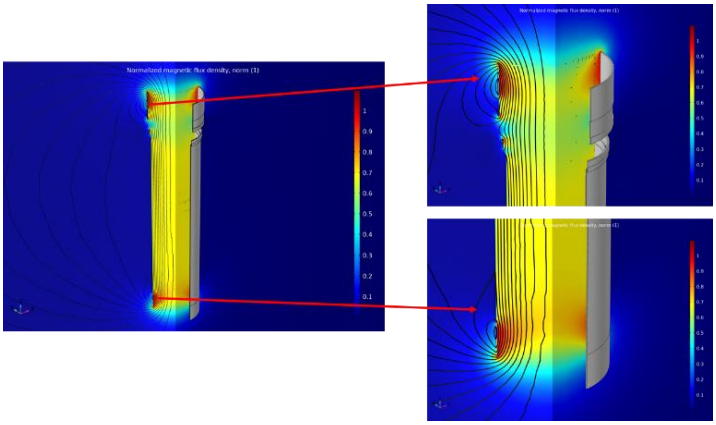

Figure 5. Non-dimensioned norm of the magnetic field

Even if the results are normalized, Figure 6 shows that the z-component of the magnetic field is much higher than the r one. Indeed, this component is nearly equal to the norm of the field. Therefore, the computations provide the classical result of the magnetic field in a solenoid in that case.

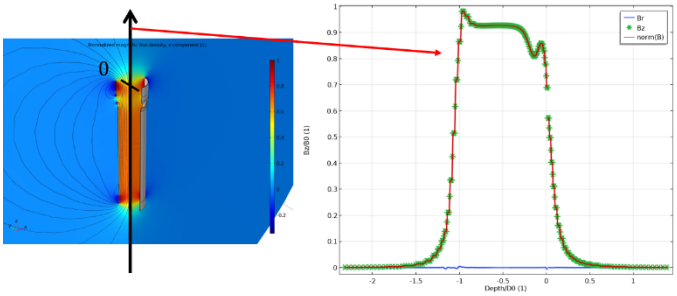

Figure 6: Comparison between all the components of the magnetic field

Experimental measurements for different intensities were performed inside the furnace to quantify the magnetic field, and to estimate the validity of the model. Figure 7 shows a good correlation between experimental measurements and numerical results: the average of the deviation between calculated and experimental values is around 7%.

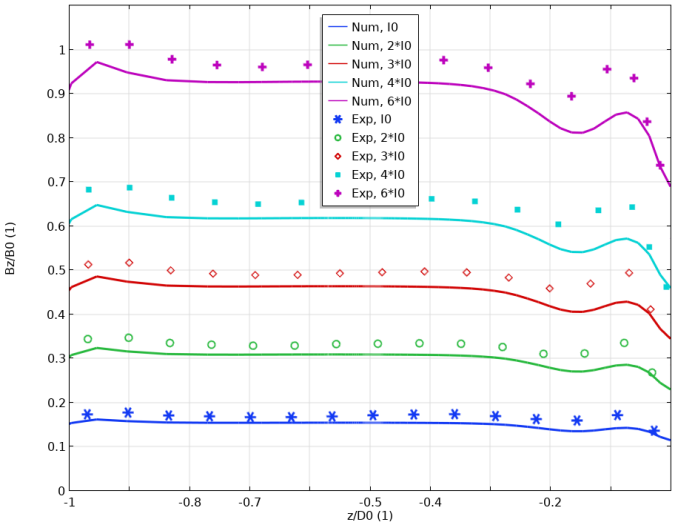

Figure 7: Comparison between experimental measurements and numerical computations of the z-component of the magnetic field.

It is worth noticing that the two experimental extrema, at the top and at the bottom of the furnace, can be found numerically. The small differences obtained especially for high intensities could be explained by the modeling assumptions and/or experimental inaccuracies.

With the electrode and the ingot

The current density is now applied in the top of the electrode and the resulting electromagnetic field is computed. The electric potential is plotted in Figure 8. Electrical conductivities in the electrode (red area) and the ingot (blue area) are very high compared to those of the arc domain. Therefore, a sharp gradient of the electric potential is obtained in this area, depending on the distance between the ingot and the electrode as well as the arc electrical conductivity.

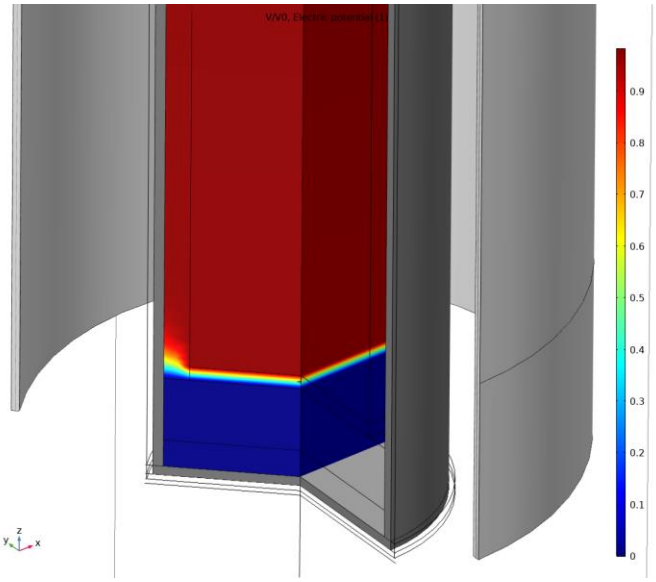

Figure 8: Non-dimensioned electric potential in the electrodes and in the surrounding vacuum

Due to the combination of the electric current flowing through the system and the magnetic field generated by the coil, Lorentz forces are generated in the three directions of space. Their mathematical formulation is given here:

$$\boldsymbol{F_{EM}} = \boldsymbol{J} \times \boldsymbol{B} = \begin{Bmatrix} -j_z^{electr} B_\phi^{electr} \\ j_z^{electr} B_r^{ind} - j_r^{electr} B_z^{ind} \\ j_r^{electr} B_\phi^{electr} \end{Bmatrix}_{r,\phi,z} \qquad Eq.\ 4$$

An accurate evaluation of these forces is determinant to understand and control the melt pool behavior. An illustration of the resulting force field is shown in Figure 9. The major part of the field applies in the phi-component, generated by the combination of the electric field generated by the electrode and the magnetic field generated by the coil.

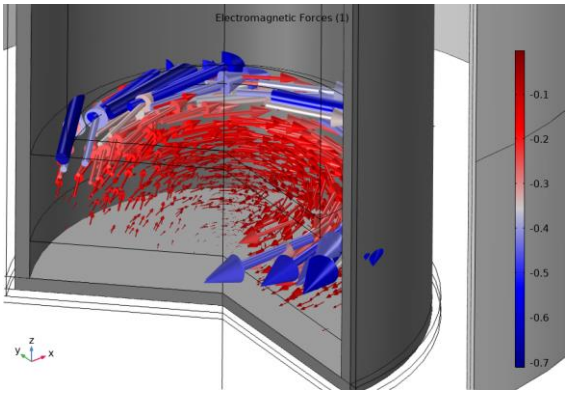

Figure 9: Non-dimensioned norm of the Lorentz force field (color) and Lorentz forces in arrows

By changing the sign of the current in the coil, and thus the orientation of the magnetic field, different modes of stirring can then be performed. This will largely affect the molten metal behavior and thus the quality of the whole process.

Conclusions

This work enables to find with a good accuracy level the experimental results concerning the magnetic field. The r-component of the magnetic field is negligible compared to the z-component. The coupling between the electric current flowing in the electrode and the ingot and the magnetic field generated by the coils has been studied. Finally, the resulting Lorentz forces have been computed to understand and better control the stirring during the process. The good agreement between calculations and experiments validates the first step of a larger R&D program. The next step is the use of this predictive model to propose process optimization or new designs of the coils.

References

1. Materials Handbook - Chp 4 : Less Common Nonferrous Metals (2008)
2. A. Jardy ; F. Leclerc, M. Revil-Baudard, P. Guerin, H. Combeau, V. Rebeyrolle – Journal of ASTM International al.7 (2010) 1-17
3. P.O.Delzant, B. Baque, P. Chapelle, A.Jardy, Metallurgical and Materials Transactions B, (2018), vol. 49, n° 3, pp. 958-968